Quantum Information Processing manuscript No.
(will be inserted by the editor)

Exciton-mediated quantum search on a star graph

Vincent Pouthier

Received: date / Accepted: date

Abstract A fast and efficient quantum search algorithm is established by using the ability of an exciton to propagate along a star graph that exhibits two identical energetic defects. The first defect lies on the well-defined input site where the exciton is initially created whereas the second defect occupies the target site whose unknown position must be determined. It is shown that when the energetic defects are judiciously chosen, specific quantum interferences arise so that the probability to observe the exciton on the target site becomes close to unity at a very short time t^*. Consequently, a measurement of the exciton quantum state at time t^* will reveal the identity of the position of the target site. The key point is that t^* is the shortest time independent on the size of the graph that is physically accessible to the exciton to tunnel.

Keywords Exciton · Star Graph · Quantum search · Quantum walk

1 Introduction

Quantum computer science was born in the early 80's through the pioneer reflection of famous researchers like Richard Feynman [1] and David Deutsch [2]. However, it was not until the mid-90's that one was able to really appreciate its powerfulness through the development of efficient quantum algorithms. One of the most famous example is probably the algorithm of Peter Shor [3,4] to factoring a large integer, i.e. a key procedure involved in many cryptographic protocols. While it is estimated that many billions of billions of years are needed to factorize an integer involving thousand numbers using a classical computer, this operation would require a few dozen minutes with a quantum computer.

Another famous quantum algorithm was developed by Lov Grover [5,6] to solve computational search problems. More precisely, this algorithm is usually described as a powerful way to find a marked item within an unsorted database involving N_0 items. While a classical computer takes $O(N_0)$ steps to find the target element

V. Pouthier
Institut UTINAM, Université de Franche-Comté, CNRS UMR 6213, 25030 Besançon, France.
E-mail: vincent.pouthier@univ-fcomte.fr

with a constant probability, the Grover's algorithm suggests that only $O(\sqrt{N_0})$ steps are needed to a quantum computer, the required storage space scaling as $O(logN_0)$. This remarkable $\sqrt{N_0}$ speedup illustrates the overwhelming superiority of quantum computation that originates in the interplay between quantum parallelism, quantum superposition of states and quantum interferences.

The Grover's algorithm, and its generalizations, can be applied to a broad range of problems so that different strategies have been developed to implement quantum search algorithms (see for instance Refs. [7–9]). In particular, following the pioneer works of Farhi and Gutmann [10], it has been suggested by Childs and Goldstone [11] that continuous time quantum walks (CTQW) on complex networks provide a natural way for performing quantum searches. Note that other approaches were also considered, involving for instance discrete time quantum walks [12–16] and nonlinear quantum walks [17,18]. On a complex network, the linked nodes define the items and the corresponding graph accounts for the local nature of the unstructured database. A target node with specific properties defines the marked item whose position must be determined as fast as possible. To realize this spatial search, CTQW-based method proceeds as follows. First, the dynamics of the quantum walker is controlled by an Hamiltonian $H = \Phi L + \Delta H$, where Φ is the hopping constant between the linked nodes, L is the so-called Laplacian matrix [19] and ΔH is a perturbation localized on the target node known as the Hamiltonian oracle [10]. Then, initially uniformly distributed over the whole network, the quantum state of the walker freely evolves under the influence of the Hamiltonian H. Therefore, when the hopping constant Φ is judiciously chosen, the quantum state suddenly localizes on the target node for a specific time t^*. Finally, a measurement of the quantum state at time t^* will find the walker localized on the target node, hence revealing the identity of its position. Within this approach, the so-called $\sqrt{N_0}$ speedup occurs on a complete graph and on cubic graphs whose dimension d is larger than 4 [11]. Unfortunately, in low-dimensional cubic graphs ($d \leq 3$), the search algorithm does not provide substantial speedup, a negative feature that has been observed also on fractal networks by Mulken and co-workers [20].

In this paper, following the original idea of Thilagam [21], we introduce a new spatial search algorithm based on the ability of an exciton to propagate along a molecular network. Such an approach is not the result of chance since recent investigations have revealed that exciton-mediated quantum state transfer could be a promising way for quantum information processing in nanowires [22,23], tree-like molecules [24–27] and star graphs [28]. The protocol we propose differs from previous search algorithms for at least three main reasons. First, as a physical realization of a CTQW, the excitonic dynamics is governed by a tight-binding Hamiltonian. Its diagonal part corresponds to the so-called site energies that differ from the site degrees which enter the definition of the Laplacian matrix. As a result, a different dynamical behavior is expected to occur. Second, instead of being delocalized over the whole network, we consider a situation in which the exciton is initially localized on a particular site called the input site. As time elapses, we aim that the exciton reaches a specific site, namely the target site, whose position is unknown. A final measurement is supposed to find the exciton on the target site, hence revealing its position. Finally, the key point is that the input site and the target site correspond to energetic defects whose site energy is shifted by an amount Δ. The proposed algorithm is thus based on the optimization

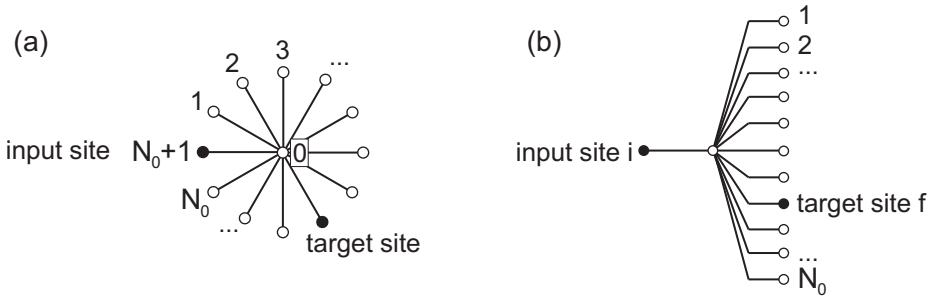

Fig. 1 (a) Representation of a star graph S_{N_0+1} with N_0+2 sites and N_0+1 branches that exhibits two defects. (b) Equivalent representation involving an input site connected to N_0 output sites through a central node. These output sites form the database and the target site defines the marked item whose position must be find.

of the Δ value so that an efficient spatial search takes place as fast as possible. Consequently, we do not need to optimize the hopping constant, a procedure that seems difficult to implement at a molecular level because it requires to reorganize the architecture of the network in order to modify the links between the connected nodes.

To illustrate how the present algorithm operates, we consider the exciton dynamics on a star graph [28–32]. This graph is one of the most regular structures in graph theory. Organized around a central core, it exhibits the local tree structure of irregular and complex networks. However, its topology remains sufficiently simple so that analytical calculations can be carried out exactly. This work can thus be viewed as a first step and more realistic situations will be addressed in forthcoming papers.

The present paper is organized as follows. In Sect. 2, the star graph we consider is introduced and the proposed quantum search algorithm is described. Then, one specifies the exciton Hamiltonian and one defines the so-called success probability, that is the probability that the exciton tunnels efficiently between the input site and the target site. In Sect. 3, a numerical simulation is carried out to study the time evolution of the success probability and to define the optimal situation for which a fast quantum search takes place. Finally, in Sect. 4, these numerical results are discussed and interpreted.

2 Theoretical background

2.1 Factual background

The system we consider is the star graph S_{N_0+1} illustrated in Fig. 1a. It defines a molecular tree involving N_0+2 sites and formed by N_0+1 branches that emanate out from a central core. The central site is thus connected to N_0+1 branch sites. Each site is occupied by a molecular subunit whose internal dynamics is described by a two-level system. Among the N_0+2 subunits, N_0 sites are occupied by equivalent two-level systems whose Bohr frequency is denoted ω_0. The last two sites are occupied by different subunits that correspond to energetic defects, the Bohr frequency of which referred as $\omega_0' = \omega_0 + \Delta$ being shifted by an amount Δ.

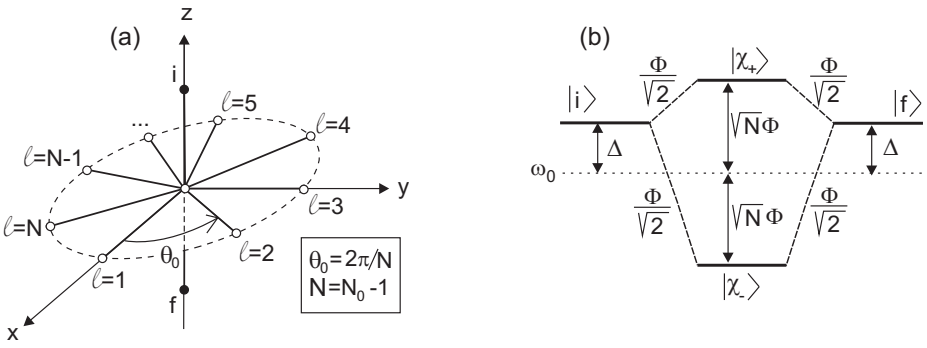

Fig. 2 (a) Representation of two defect sites i and f connected to the central core of a star graph S_N with $N = N_0 - 1$. (b) Representation of the restricted Hamiltonian $\mathcal{H}$ that governs the exciton dynamics when the input site is initially excited (see the text).

The first defect stands for the input site i whose position is well-defined whereas the second defect occupies the so-called target site f whose position is unknown. Although, the system clearly refers to a star graph, its symmetric nature allows us to represent the network as an input site i connected to N_0 output sites through a central node. Therefore, as shown in Fig. 1b, these output sites can be viewed as a database so that the target site f defines the marked item whose unknown position must be find as fast as possible.

As outlined in the introduction, to realize such a spatial search one proposes the following quantum protocol. At time $t = 0$, the two-level system located on the input site i is excited resulting in the creation of an exciton. As time elapses, this exciton propagates along the star according to the hopping constant Φ that connects the linked nodes thus performing a physical realization of a CTQW. In that context, the parameter Δ must be judiciously optimized so that there exists a very short time t^* for which the probability that the exciton occupies the target site f is maximum. Finally, a measurement of the excitonic quantum state is performed at time t^*. If the optimization step is successful, the result of this experiment will give the location of the exciton, thus revealing the most probable position of the target site.

So defined, our protocol clearly shows that the central object of the present study is the success probability $P_{fi}(t)$, that is the probability to observe the exciton at time t on the target site f given that it was initially on the input site i. Owing to the star symmetry, the success probability does not depend on the position of the target site. Therefore, one can arbitrary fix the position of the target site to study the time evolution of the success probability, hence defining both the optimized Δ value and the time t^* required to establish the desired quantum search protocol.

2.2 Model Hamiltonian

For evaluating the success probability, we can take advantage of the fact that the network under study can be viewed as two defect sites i and f connected to the central core of a star graph S_N, with $N = N_0 - 1$. This point of view is illustrated in Fig. 2a. The graph S_N involves N branch sites $\ell = 1, ..., N$ that encircle a

central core $\ell = 0$. According to the previous description, each site is occupied by a two-level system and one defines $|\ell\rangle$ as the state in which the ℓth two-level system lies in its first excited state, the other two-level systems remaining in their ground state. Similarly, let $|i\rangle$ and $|f\rangle$ denote the excited states localized on the input site i and on the target site f, respectively.

Within the local basis $\{|i\rangle, \{|\ell\rangle\}_{\ell=0,...,N}, |f\rangle\}$, the exciton dynamics is governed by a tight-binding Hamiltonian written as (the convention $\hbar = 1$ will be used throughout this paper)

$$H = \sum_{\ell=0}^{N} \omega_0 |\ell\rangle\langle\ell| + (\omega_0 + \Delta)(|i\rangle\langle i| + |f\rangle\langle f|) + \sum_{\ell=1}^{N} \Phi(|0\rangle\langle\ell| + |\ell\rangle\langle 0|) + \Phi(|0\rangle\langle i| + |i\rangle\langle 0|) + \Phi(|0\rangle\langle f| + |f\rangle\langle 0|) \quad (1)$$

where Φ is the hopping constant that connects the linked sites. This Hamiltonian can be expressed in an improved way by performing a specific Bloch transformation [28] that allows us to diagonalize the Hamiltonian of the isolated state graph S_N. Indeed, S_N possesses discrete rotational symmetry. It remains invariant under the discrete rotation of angle $\theta_0 = 2\pi/N$ and centered on the core site $\ell = 0$. As a result, one can introduce the so-called Bloch basis [33] that involves the local state $|\ell = 0\rangle$ and N orthogonal Bloch states $|\chi_k\rangle$ $(k = 1, ..., N)$ defined as

$$|\chi_k\rangle = \frac{1}{\sqrt{N}} \sum_{\ell=1}^{N} e^{ik\ell\theta_0} |\ell\rangle \quad (2)$$

Within the Bloch basis, S_N exhibits two kinds of eigenstates. First, the spectrum of the graph shows the $(N-1)$-fold degenerate eigenenergy ω_0, the corresponding eigenstates being the $N-1$ Bloch states $|\chi_k\rangle$, with $k = 1, ..., N-1$. Second, the graph supports two eigenstates $|\chi_\pm\rangle$ that correspond to superimpositions involving the state $|0\rangle$ and the Bloch state $|\chi_N\rangle$ that is uniformly distributed over the periphery of the star. These totally symmetric eigenstates are defined as

$$|\chi_\pm\rangle = \frac{1}{\sqrt{2}}(|0\rangle \pm |\chi_N\rangle) \quad (3)$$

the corresponding eigenenergy being $\omega_\pm = \omega_0 \pm \sqrt{N}\Phi$. Consequently, within the basis $\{|i\rangle, \{|\chi_k\rangle\}_{k=1,...,N-1}, |\chi_\pm\rangle, |f\rangle\}$, the exciton Hamiltonian is rewritten as

$$H = \sum_{k=1}^{N-1} \omega_0 |\chi_k\rangle\langle\chi_k| + \sum_{\sigma=\pm} \omega_\sigma |\chi_\sigma\rangle\langle\chi_\sigma| + (\omega_0 + \Delta)(|i\rangle\langle i| + |f\rangle\langle f|) + \sum_{\sigma=\pm} \left[\frac{\Phi}{\sqrt{2}}(|\chi_\sigma\rangle\langle i| + |i\rangle\langle\chi_\sigma|) + \frac{\Phi}{\sqrt{2}}(|\chi_\sigma\rangle\langle f| + |f\rangle\langle\chi_\sigma|) \right] \quad (4)$$

According to Eq.(4), the defect states $|i\rangle$ and $|f\rangle$ interact only with the totally symmetric star states $|\chi_\pm\rangle$. Therefore, when the exciton is initially created on the input site i, its dynamics remains confined in an active subspace spanned by the four vectors $\{|i\rangle, |\chi_+\rangle, |\chi_-\rangle, |f\rangle\}$. In this active subspace, the propagation

of the exciton is thus governed by the restricted Hamiltonian $\mathcal{H}$ whose matrix representation is expressed as

$$\mathcal{H} = \begin{pmatrix} \omega_0 + \Delta & \frac{\Phi}{\sqrt{2}} & \frac{\Phi}{\sqrt{2}} & 0 \\ \frac{\Phi}{\sqrt{2}} & \omega_0 + \sqrt{N}\Phi & 0 & \frac{\Phi}{\sqrt{2}} \\ \frac{\Phi}{\sqrt{2}} & 0 & \omega_0 - \sqrt{N}\Phi & \frac{\Phi}{\sqrt{2}} \\ 0 & \frac{\Phi}{\sqrt{2}} & \frac{\Phi}{\sqrt{2}} & \omega_0 + \Delta \end{pmatrix}. \tag{5}$$

So defined, $\mathcal{H}$ clearly refers to a four-level system whose characteristics are displayed in Fig. 2b.

2.3 Success probability

In the active subspace, the exciton dynamics is described by the evolution operator $U(t)$, whose behavior is governed by the Schrodinger equation, as

$$i\frac{\partial U(t)}{\partial t} = \mathcal{H}U(t) \tag{6}$$

The solution of Eq.(6) yields the so-called transition amplitudes that provide key information on the ability of the exciton to tunnel along the network. In particular, the probability amplitude for observing the exciton on the target site f at time t given that it occupied the input site i at time $t = 0$ is defined by the matrix element $U_{fi}(t)$. This element can be determined easily by diagonalizing the system Hamiltonian Eq. (5). Let $|\Psi_\alpha\rangle$ denote the αth eigenstate of $\mathcal{H}$ and $\hat{\omega}_\alpha$ the corresponding eigenvalue, with $\alpha = 1, 2, 3, 4$. The probability amplitude is expressed in terms of the stationary wave functions $\Psi_{\alpha k} = \langle k|\Psi_\alpha\rangle$ with $k = i, f$ as

$$U_{fi}(t) = \sum_{\alpha=1}^{4} \Psi_{\alpha,f}\Psi^*_{\alpha,i}e^{-i\hat{\omega}_\alpha t} \tag{7}$$

In accordance with the laws of quantum mechanics, this amplitude is the sum over the elementary amplitudes associated with the different paths that the exciton can follow to tunnel. A given path defines a transition through a stationary state $|\Psi_\alpha\rangle$ and it exhibits two contributions. First, it involves the weight of the localized states $|i\rangle$ and $|f\rangle$ in the stationary state $|\Psi_\alpha\rangle$. Then, it depends on a phase factor that accounts for the free evolution of the exciton.

In that context, the success probability, that is the probability that the exciton reaches the target site at time t provided that it was localized on the input site at time $t = 0$ is defined as

$$P_{fi}(t) = |U_{fi}(t)|^2 \tag{8}$$

The time evolution of $P_{fi}(t)$ results from the interferences between the paths that the exciton can follow to tunnel from the input site to the target site. As shown in the following of the text, our aim is thus to control these interferences by varying the value of the Δ parameter in order that the success probability reaches a significant value as fast as possible.

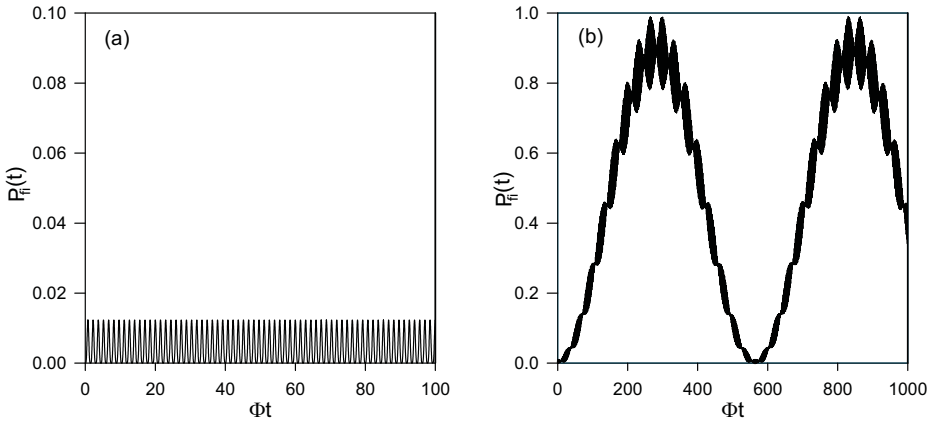

Fig. 3 Time evolution of the success probability for $N = 16$ and for **a** $\Delta = 0.0$ and **b** $\Delta = 0.1\Phi$.

3 Numerical Results

In this section, the previous formalism is applied for studying the time evolution of the success probability for different Δ values and for different N values. To proceed, the two-level Bohr frequency will stand for the energy reference, i.e. $\omega_0 = 0$.

For very small Δ values, the time evolution of the success probability is displayed in Fig. 3 for $N = 16$. When $\Delta = 0$, $P_{fi}(t)$ oscillates periodically between its initial value equal to zero and a maximum value whose amplitude reaches 1.20% (see Fig. 3a). Note that the period of these oscillations is approximately equal to $1.48\Phi^{-1}$. A fully different behavior occurs when $\Delta = 0.1\Phi$, as displayed in Fig. 3b. The success probability behaves as a slowly varying function that supports a high-frequency small-amplitude modulation. This high-frequency component, whose period is approximately equal to $1.4\Phi^{-1}$, clearly refers to the small-amplitude oscillations observed in the limit $\Delta = 0$. By contrast, the low-frequency component, whose period is about $565\Phi^{-1}$, scales as a sine-like function that reaches a maximum value quite close to unity. Over the time scale considered here, this maximum is equal to 99.16% and it arises at time $t = 265.83\Phi^{-1}$. These features indicate that a non-vanishing Δ value favors an efficient transfer between the input site and the target site. However, this transfer takes place for a quite long time.

As shown in Fig. 4a, a similar behavior occurs for larger Δ values, provided that $\Delta < \Phi$. Nevertheless, the frequency of the slowly varying component increases as Δ increases so that the success probability reaches a significant value at a time that decreases with Δ. For instance, the first significant success probability that is quite close to unity occurs at times $t \approx 132.53\Phi^{-1}$, $65.87\Phi^{-1}$ and $27.35\Phi^{-1}$ when $\Delta = 0.2\Phi$, 0.4Φ and Φ, respectively. Note that the occurrence of the maximum maximorum of $P_{fi}(t)$ depends on the value of the observation time. For instance, for $\Delta = \Phi$, the maximum reached by the success probability at time $t = 27.35\Phi^{-1}$, equal to 98.09%, corresponds to a local maximum. In fact, over the time scale considered on the figure, the maximum maximorum takes place at time $t \approx 80.50\Phi^{-1}$, the corresponding value being equal to 98.79%. As Δ increases, the amplitude of the high-frequency modulation increases, as observed in Fig. 4b for $\Delta = 3.0\Phi$. In that case, $P_{fi}(t)$ rapidly reaches a local maximum whose value is equal to 98.95%,

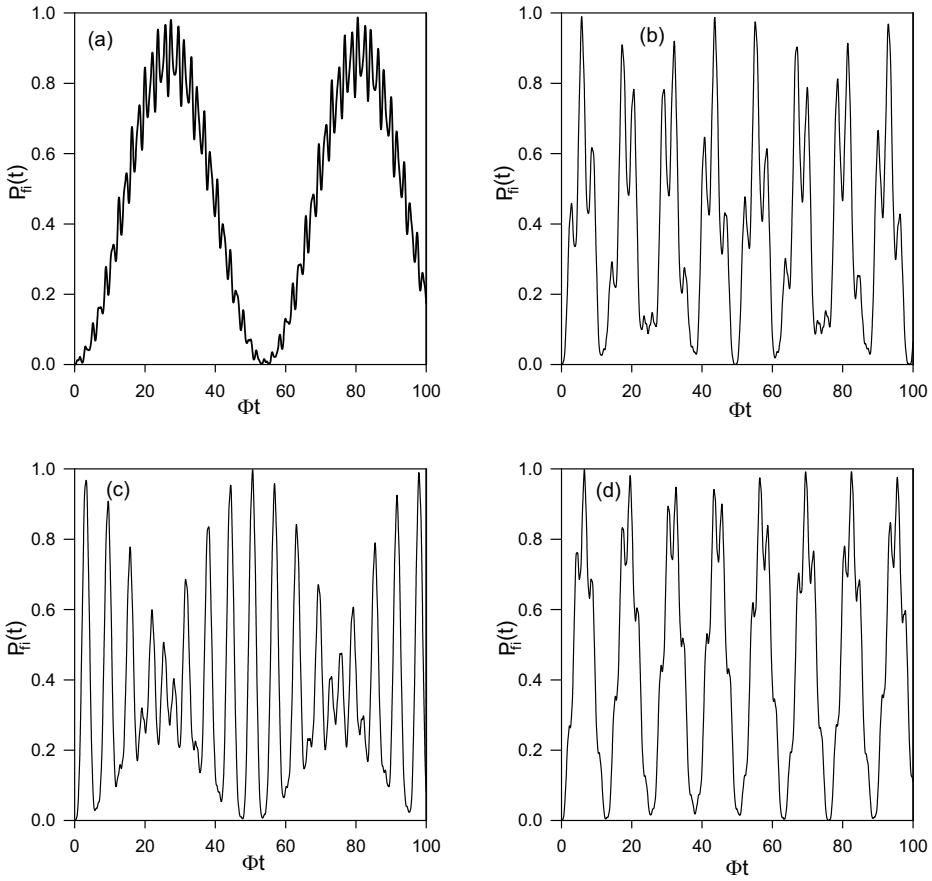

Fig. 4 Time evolution of the success probability for $N = 16$ and for **a** $\Delta = \Phi$, **b** $\Delta = 3.0\Phi$, **c** $\Delta = 4.0\Phi$ and **d** $\Delta = 6.0\Phi$.

this maximum occurring for a quite short time $t = 5.76\Phi^{-1}$. Then, for $\Delta = 4.0\Phi$, a particular situation takes place, as displayed in Fig. 4c. The two spectral components involved in the success probability can be clearly distinguished. Therefore, similarly to what happens in amplitude modulation technique, $P_{fi}(t)$ behaves as a high-frequency carrier wave multiplied by a low-frequency modulation waveform. Although it reaches a significant value equal to 96.76% at the very short time $t = 3.28.\Phi^{-1}$, its maximum value equal to 99.77% occurs at a longer time $t = 50.60\Phi^{-1}$, over the time scale considered here. Finally, for larger Δ values, a slowly sine-like function dressed by small-amplitude high-frequency oscillations recurs, as illustrated in Fig. 4d. For $\Delta = 6.0\Phi$, the maximum value of the success probability, equal to 99.79%, arises at $t = 6.52\Phi^{-1}$. In fact, in that regime, the frequency of the slowly varying component decreases as Δ increases so that $P_{fi}(t)$ reaches a local maximum value close to unity at a time that increases with Δ.

A detailed analysis of the time evolution of the success probability reveals the occurrence of a critical Δ value approximately equal to $\Delta^* \approx 4.12\Phi$ for $N = 16$. When $\Delta \approx \Delta^*$, the two spectral components that define the success probability

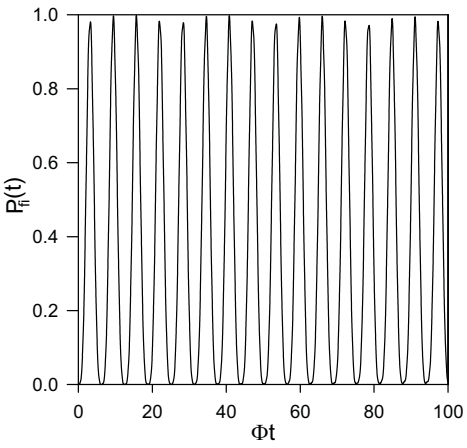

Fig. 5 Time evolution of the success probability for $N = 16$ and for $\Delta = 4.12\Phi$.

exhibit almost the same amplitude. Consequently, as shown in Fig. 5, $P_{fi}(t)$ behaves as a sine-like function that varies almost periodically between zero and a maximum very close to unity, the corresponding period being approximately equal to $6.24\Phi^{-1}$. At a very short time $t = 3.26\Phi^{-1}$, $P_{fi}(t)$ reaches a local maximum equal to 98.11% indicating that a very fast efficient transfer arises between the input site and the target site, as required to obtain an optimized powerful quantum search algorithm. Note that over the time scale considered here, the maximum maximorum of the success probability arises at time $t = 15.66\Phi^{-1}$ and it is equal to 99.80%.

Over an observation time scale fixed to $T_{obs} = 100\Phi^{-1}$, let P_{max} define the maximum value of the success probability and let t_{max} denote the time for which this maximum occurs. The Δ dependence of both P_{max} and t_{max} is illustrated in Fig. 6 for $N = 16$.

As shown in Fig. 6a, the efficiency of the transfer is very poor for small Δ values and P_{max} becomes significant provided that $\Delta > 0.23\Phi$. In fact, the behavior for very small Δ values corresponds to a numerical artifact that arises because the observation time is finite, that is the maximum maximorum is expected to occur after T_{obs}. When $\Delta > 0.23\Phi$, the maximum value of the success probability remains typically larger than 95%, indicating that the transition of the exciton on the target site is a very likely event. Note that P_{max} becomes larger than 99.99% for many Δ values such as $\Delta = 4.32\Phi$, 5.04Φ and 6.19Φ, to cite a few. In that specific cases, one is practically certain to observe the exciton on the target site for a time shorter than T_{obs}. Nevertheless, for specific Δ values, the curve $P_{max}(\Delta)$ exhibits holes for which the maximum value of the success probability sightly decreases. For instance, it reduces to 75.50% for $\Delta = 3.46\Phi$ and 4.85Φ whereas it is approximately equal to 90.0% for $\Delta = 2.80\Phi$, 3.73Φ, 4.53Φ and 5.72Φ.

The Δ dependence of the time t_{max} is shown in Fig. 6b. In a general way, the various points that form the figure draw a set of similar curves whose origin can be understood as follows. As observed previously, the success probability exhibits two spectral components. It involves a low-frequency component that periodically reaches a significant value quite close to unity dressed by high-frequency small-

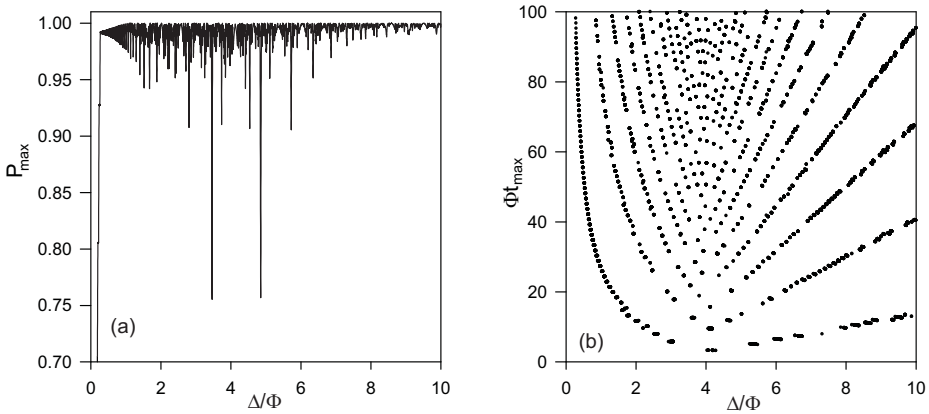

Fig. 6 **a** Δ dependence of the maximum value of the success probability P_{max} for $N = 16$. **b** Δ dependence of the time t_{max} for which the success probability reaches its maximum value for $N = 16$. The observation time is fixed to $T_{obs} = 100\Phi^{-1}$.

amplitude oscillations. Therefore, depending on the value of the parameter Δ, the high-frequency can be shifted so that the maximum maximorum of $P_{fi}(t)$ can basically correspond to either the first, the second, the third ... local maximum of the slowly varying component, thus drawing the set of curves. For each curve, a critical parameter quite close $\Delta^* \approx 4.0\Phi$, discriminates between two regimes. When $\Delta < \Delta^*$, the time t_{max} decreases with Δ according to the invert law $t_{max} \propto 1/\Delta$. By contrast, when $\Delta > \Delta^*$, t_{max} increases almost linearly with Δ. In that context, the function $t_{max}(\Delta)$ reaches its minimum when $\Delta \approx \Delta^*$. Nevertheless, the characterization of the critical region is not so easy because the various curves are not well-defined in the neighborhood of the critical point. If one considers the lowest curve, that is the curve that provides the shortest time t_{max}, the critical point corresponds approximately to $\Delta^* \approx (4.10 \pm 0.1)\Phi$. In that case, the time $t_{max} \approx 3.26\Phi^{-1}$ reaches a minimum value for which the success probability, larger than 98%, remains very important.

At this step, by performing the previous studies for different N values, we have clearly observed the occurrence of a critical parameter $\Delta^*(N)$ that is slightly larger than $\sqrt{N}\Phi$. Whatever N, this critical value discriminates between two regimes, as observed in Fig. 6. Moreover, when $\Delta \approx \Delta^*(N)$, the success probability behaves as in Fig. 5 and it shows almost periodic oscillations between zero and a maximum value very close to unity. In that context, we thus define $\Delta^*(N)$ as the critical Δ value that maximizes the amplitude of the first local maximum of the success probability and that minimizes the time at which this maximum arises. Let $P^*(N)$ denote the optimized value of this first maximum and $t^*(N)$ stand for the time for which this maximum occurs.

The N dependence of the critical parameter $\Delta^*(N)$ is displayed in Fig. 7. The figure shows that Δ^* increases with N. In quite good agreements with the results displayed in Figs. 5 and 6, one obtains $\Delta^* = 4.145\Phi$ for $N = 16$. For quite small N values, the critical parameter is slightly larger than $\sqrt{N}\Phi$. For instance, it is equal to $\Delta^* = 3.042\Phi$, 4.017Φ and 5.012Φ for $N = 8$, 15 and 24, respectively. In fact, it turns out that the critical point scales as $\Delta^*(N) \approx \sqrt{N+1}\Phi$, as illustrated in the inset of the figure. Quite good for small N values, this law is becoming better

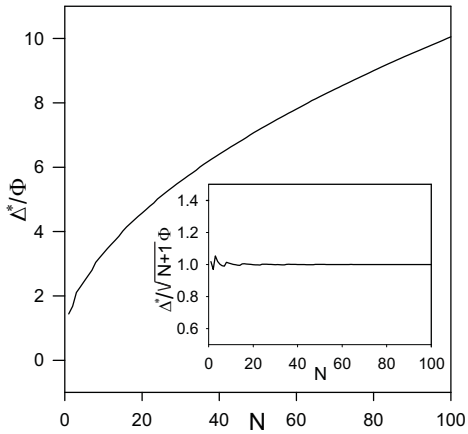

Fig. 7 N dependence of the critical parameter $\Delta^*(N)$. The inset displays the N dependence of the ratio $\Delta^*(N)/\sqrt{N+1}\Phi$.

and better as N increases. For instance, one obtains $\Delta^* = 7.004\Phi$ and 10.002Φ for $N = 48$ and 99, respectively.

At the critical point, i.e. when $\Delta = \Delta^*(N)$, the N dependence of the largest amplitude $P^*(N)$ of the first maximum reached by the success probability is shown in Fig. 8a (full circles). Note that the red dashed curve accounts for theoretical calculations that will be discussed in the next section. In a general way, the optimized probability $P^*(N)$ exhibits damped oscillations around an average value that lies just below unity. Note that this mean value is equal to 99.29% over the N range considered here. However, as N increases, the amplitude of these oscillations decreases indicating that $P^*(N)$ tends to unity when N tends to infinity. The smallest $P^*(N)$ value, equal to 88.47%, arises for $N = 3$. By contrast, the largest $P^*(N)$ value, equal to 99.99%, arises for several N values equal to $N = 29$, 41, 55, 77 and 89, respectively. Finally, provided that $N \geq 9$, the figure clearly shows that $P^*(N)$ remains larger than 96.88% indicating that the transition of the exciton from the input site to the target site is a very likely event at the critical point.

The N dependence of the time $t^*(N)$ for which the first local maximum of the success probability occurs at the critical point is displayed Fig. 8b (full circles). As previously, the red dashed curve accounts for theoretical calculations that will be discussed in the next section. As N increases, the time $t^*(N)$ shows damped oscillations around an average value approximately equal to $3.12\Phi^{-1}$. The smallest $t^*(N)$ value, equal to $2.72\Phi^{-1}$, arises for $N = 2$ whereas the largest $t^*(N)$ value, equal to $3.33\Phi^{-1}$, takes place for $N = 3$. Provided that $N \geq 9$, the figure reveals that the dispersion of the $t^*(N)$ values decays so that $t^*(N) \approx (3.12 \pm 0.16)\Phi^{-1}$. In that case, the curve t^* vs N shows a series of almost continuous variations that are separated by discontinuities that take place for specific N values equal to $N = 14$, 23, 34, 47, 62 and 98. For instance, between $N = 47$ and $N = 48$, $t^*(N)$ realizes a jump from $3.05\Phi^{-1}$ to $3.18\Phi^{-1}$ whereas it varies from $3.19\Phi^{-1}$ to $3.18\Phi^{-1}$ when N increases from 50 to 51. Nevertheless, disregarding these features, it turns out that two fundamental points arise at the critical point. First, the time required to the exciton to tunnel from the input site to the target site with a quite large

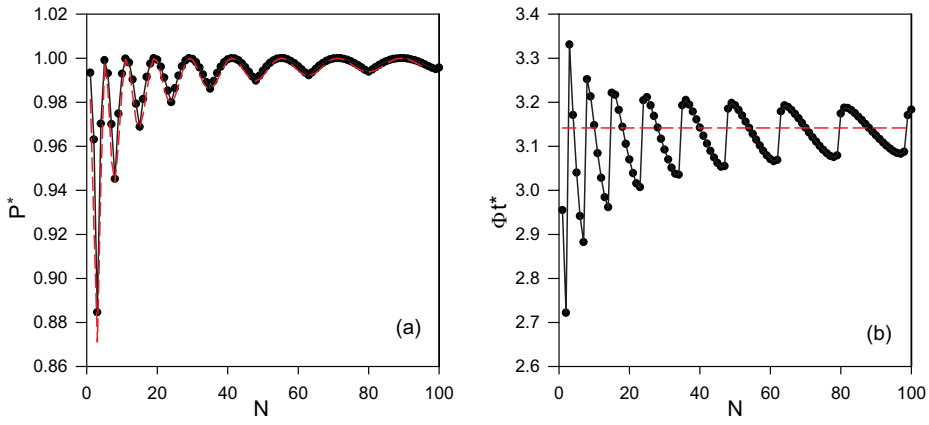

Fig. 8 **a** N dependence of the amplitude P^* of the first local maximum of the success probability at the critical point. **b** N dependence of the time t^* for which the first local maximum of the success probability occurs at the critical point.

probability is almost N independent. Second, this specific time corresponds to a very short time approximately equal to π/Φ.

4 Discussion

The numerical results clearly show that the success probability exhibits four different dynamical behaviors depending on the value of the Δ parameter. Indeed, when $\Delta = 0$, the input site and the target site are identical to the other sites. Therefore, the network corresponds to a star graph involving $N+2$ branches that emanate out from a central node. In such a system, it is well-known that a localization occurs when the exciton is initially located on a branch site so that the success probability remains very small, such an effect being enhanced as the branch number increases [28,34]. In that case, no efficient transfer arises between the input site and the target site preventing the occurrence of any successful quantum search. By contrast, an efficient tunneling arises for small non vanishing Δ values, i.e. provided that $\Delta \ll \sqrt{N}\Phi$. The success probability behaves as a slowly varying sine-like function that supports small-amplitude high-frequency oscillations. It thus reaches an important value quite close to unity, this maximum occurring over a quite long time scale that becomes shorter and shorter as Δ increases. Note that although such a situation can be exploited for realizing an efficient quantum search, the time required for a successful search is clearly too long. A similar behavior arises for large Δ values, i.e. provided that $\Delta \gg \sqrt{N}\Phi$. In that case, the success probability still exhibits two spectral components, that is a low frequency sine-like function dressed by a high-frequency small-amplitude modulation. Therefore, it reaches a significant value over a quite long time scale that decreases as Δ decreases. Once again, although an efficient quantum search can be obtained within this case, the time required for a successful search is still too long. Finally, our results have clearly shown the occurrence of a critical Δ value approximately equal to $\Delta^* \approx \sqrt{N+1}\Phi$. In that case the two spectral components that enter the definition of the success probability have almost the same amplitude so that

$P_{fi}(t)$ behaves as a short period sine-like function that varies between zero and a maximum very close to unity. Consequently, at the critical point, a very efficient transfer arises between the input site and the target site. But the key point is that this transfer occurs over a very short time scale that is approximately equal to $t^* \approx \pi/\Phi$ whatever N. One thus obtains a powerful search algorithm whose efficiency is almost independent on the size of the database.

To interpret the previous observations, both approximate and exact calculations can be done by exploiting the spectrum of the restricted Hamiltonian $\mathcal{H}$ that governs the exciton dynamics. This Hamiltonian defines a four-level system displayed in Fig. 2b. Its properties depend on the interplay between the exciton hopping constant Φ and the defect energy shift Δ, giving rise to the four dynamical behaviors observed in the previous section.

4.1 The limit $\Delta \ll \sqrt{N}\Phi$

As mentioned previously, when $\Delta = 0$, the system reduces to a star graph involving $N + 2$ branches. In that case, straightforward calculations yield the success probability as [28]

$$P_{fi}(t) = \frac{4}{(N+2)^2} \sin^4\left(\frac{\sqrt{N+2}}{2}\Phi t\right) \tag{9}$$

According to Eq. (9), the success probability defines a periodic function with period $T = 2\pi/\sqrt{N+2}\Phi$ that oscillates between zero and a maximum value equal to $4/(N+2)^2$. Note that for $N = 16$, this maximum value is equal to 1.2% and $T = 1.48\Phi^{-1}$, in a perfect agreement with the results displayed in Fig. 3a. In fact, because the graph exhibits a $(N+1)$-fold degenerate eigenenergy ω_0, specific quantum self-interferences arise when the exciton is initially located on a single branch. As a result, a localization takes place so that the exciton remains confined over the excited site, preventing any efficient transfer between the input site and the target site [28,34].

For non vanishing Δ values, in the limit $\Delta \ll \sqrt{N}\Phi$, degenerate perturbation theory [35,36] can be applied for characterizing approximately the behavior of the low frequency component of the success probability. Indeed, as shown in Fig. 2b for small Δ values, the four-level system that defines the exciton Hamiltonian in the active subspace involves two degenerate energy levels associated to the defect states $|i\rangle$ and $|f\rangle$ and two energy levels associated to the totally symmetric star states $|\chi_\pm\rangle$. Because, the defect states are located far from the star states, the interaction between defect states and star states has two main consequences. First, it induces an energy correction of the defect states. Second, it favors an effective interaction between the defect states. As a result, after straightforward calculations, the effective hopping constant between the input site and the target site is expressed as

$$\hat{\Phi} = \frac{\Delta\Phi^2}{\Delta^2 - N\Phi^2} \tag{10}$$

Note that the energy correction corresponds to a shift of the Δ parameter expressed as $\Delta \to \Delta + \hat{\Phi}$.

In that context, the defect states basically form a coupled two-level system whose dynamics defines the low-frequency behavior of the success probability that approximately scales as

$$P_{fi}(t) \approx \sin^2(\hat{\Phi}t) \tag{11}$$

In a quite good agreement with the numerical results displayed in Fig. 4a, the low-frequency component of the success probability behaves as a sine-like function that periodically reaches unity, the corresponding period being equal to $\pi/\hat{\Phi}$. Consequently, when $\Delta \ll \sqrt{N}\Phi$, $P_{fi}(t)$ reaches its first maximum at time $t = \pi/(2\hat{\Phi}) \approx \pi N/(2\Delta)$. In other words, the non vanishing Δ value favors an efficient transfer between the input site and the target site, this transfer occurring over a quite long time scale that decreases as Δ increases according to an invert law, as observed in Fig. 6 b. Note that, in addition to the low frequency component Eq.(11), $P_{fi}(t)$ supports high-frequency small-amplitude oscillations that account for the localization process observed in the limit $\Delta = 0$. As a result, this modulation can shift the position of the maximum value of the success probability. The time for which the maximum arises thus draws a set of curves approximately given by $\pi N/(2\Delta)$, $3\pi N/(2\Delta)$, $5\pi N/(2\Delta)$, ... and so on, as shown in Fig. 6b.

4.2 The limit $\Delta \gg \sqrt{N}\Phi$

In the limit $\Delta \gg \sqrt{N}\Phi$, the energy diagram shown in Fig. 2b still exhibits the two degenerate energy levels associated to the defect states that are located far from the levels associated to the star states. Therefore, as previously, degenerate perturbation theory can be applied for characterizing the low frequency component of the success probability. In fact, the effective hopping constant between the input site and the target site is still written as $\hat{\Phi} = \Delta\Phi^2/(\Delta^2 - N\Phi^2)$ resulting in a low-frequency component of the success probability that still behaves as $P_{fi}(t) \approx \sin^2(\hat{\Phi}t)$. As observed in Fig. 4d, $P_{fi}(t)$ periodically reaches unity according to a period equal to $\pi/\hat{\Phi}$. It thus reaches its first maximum at time $t = \pi/(2\hat{\Phi}) \approx \pi\Delta/(2\Phi^2)$ indicating that an efficient transfer arises between the input site and the target site. Nevertheless, this transfer takes place over a long time scale that increases linearly with Δ, in a quite good agreement with the results displayed in Fig. 6 b. Note that the occurrence of a set of curves still results from the presence of the high-frequency small-amplitude oscillations in the success probability.

4.3 The critical point $\Delta = \sqrt{N+1}\Phi$

4.3.1 Approximate results

At the critical point, when $\Delta \approx \sqrt{N}\Phi$, the perturbation theory is no longer valid because a resonance occurs between the two defect states and the totally symmetric star state $|\chi_+\rangle$. Note that the physics is equivalent when one considers the case $\Delta \approx -\sqrt{N}\Phi$, a resonance occurring with $|\chi_-\rangle$.

For sufficient large N values, the problem can thus be solved approximately by disregarding the coupling between the defect states and the star state $|\chi_-\rangle$. In doing so, the restricted Hamiltonian $\mathcal{H}$ thus describes the near resonant coupled

states $|i\rangle$, $|\chi_+\rangle$ and $|f\rangle$ and the isolated unperturbed state $|\chi_-\rangle$. Under this form, $\mathcal{H}$ can be diagonalized exactly, the resulting eigenvalues being expressed as (with the convention $\omega_0 = 0$)

$$\begin{aligned}
\hat{\omega}_1 &= -\sqrt{N}\Phi \\
\hat{\omega}_2 &= \frac{\Delta + \sqrt{N}\Phi}{2} - \sqrt{\left(\frac{\Delta - \sqrt{N}\Phi}{2}\right)^2 + \Phi^2} \\
\hat{\omega}_3 &= \Delta \\
\hat{\omega}_4 &= \frac{\Delta + \sqrt{N}\Phi}{2} + \sqrt{\left(\frac{\Delta - \sqrt{N}\Phi}{2}\right)^2 + \Phi^2}
\end{aligned} \tag{12}$$

The first eigenstate $|\Psi_1\rangle = |\chi_-\rangle$ does not depend on the defect states. By contrast, the third eigenstate $|\Psi_3\rangle = (|i\rangle - |f\rangle)/\sqrt{2}$ is an antisymmetric superimposition that involves only the defect states. The remaining eigenstates $|\Psi_{2,4}\rangle$ are coherent superimpositions involving $|i\rangle$, $|\chi_+\rangle$ and $|f\rangle$, as

$$|\Psi_{2,4}\rangle = \frac{1}{\sqrt{2 + 2\frac{(\hat{\omega}_{2,4} - \Delta)^2}{\Phi^2}}} \left(|i\rangle + \frac{\sqrt{2}(\hat{\omega}_{2,4} - \Delta)^2}{\Phi^2}|\chi_+\rangle + |f\rangle\right) \tag{13}$$

In that context, the knowledge of both the eigenvectors and the eigenvalues of the Hamiltonian allows us to build the approximate expression of the evolution operator Eq.(7). Therefore, the probability amplitude to observe the exciton on the target site f at time t provided that it was on the excited site i at time $t = 0$ is written as

$$U_{fi}(t) \approx -\frac{1}{2}e^{-i\Delta t}\left(1 - \frac{e^{-i(\hat{\omega}_2 - \Delta)t}}{1 + \frac{(\hat{\omega}_2 - \Delta)^2}{\Phi^2}} - \frac{e^{-i(\hat{\omega}_4 - \Delta)t}}{1 + \frac{(\hat{\omega}_4 - \Delta)^2}{\Phi^2}}\right) \tag{14}$$

The transition amplitude is the sum over the three elementary amplitude associated to the three paths that the exciton can follow to tunnel from the input site to the output site. A specific path corresponds to a transition mediated by one of the three eigenstates $|\Psi_\alpha\rangle$, with $\alpha = 2$, 3 and 4. Therefore, each elementary amplitude involves the weight of the defect states in the stationary state $|\Psi_\alpha\rangle$ and it depends on a phase factor that accounts for the free evolution of the exciton. Consequently, the time evolution of the transition amplitude will result from the quantum interferences between the different paths, interferences whose main influence is encoded into the two Bohr frequencies $\varpi_1 = \Delta - \hat{\omega}_2$ and $\varpi_2 = \hat{\omega}_4 - \Delta$, respectively.

Depending on the relative values of the relevant Bohr frequencies, different regimes occurs resulting either in an efficient or in an inefficient transfer between the input site and the target site. To illustrate these features, Fig. 9a shows the Δ dependence of the maximum value P_{max} of the success probability $P_{fi}(t) = |U_{fi}(t)|^2$ for $N = 16$, the observation time being fixed to $T_{obs} = 100\Phi^{-1}$. The Δ dependence of the corresponding time t_{max} is shown in Fig. 9b, t_{max} defining the time for which $P_{fi}(t_{max}) = P_{max}$. Although the present approach is valid near the critical point, it turns out that the results displayed in Fig. 9 qualitatively agree with the numerical calculations shown in Fig. 6. Indeed, P_{max} remains typically larger than 95% and for specific Δ values, the curve $P_{max}(\Delta)$ reaches unity

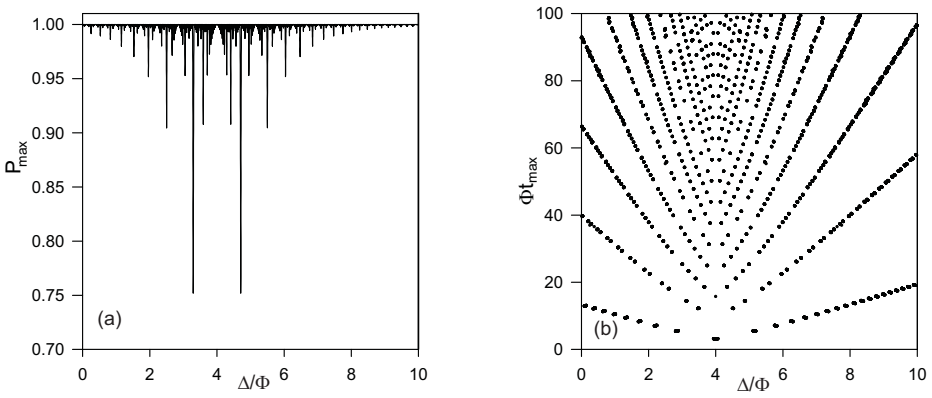

Fig. 9 **a** Δ dependence of the maximum value of the approximate success probability P_{max} for $N = 16$. **b** Δ dependence of the approximate time t_{max} for which the success probability reaches its maximum value for $N = 16$. The observation time is fixed to $T_{obs} = 100\Phi^{-1}$.

indicating that a perfect transfer arises. Nevertheless, for other specific Δ values, the curve displays holes for which the maximum value of the success probability sightly decreases. Similarly, the Δ dependence of t_{max} gives rise to a set of curves. For each curve, t_{max} first decreases with Δ until it reaches a minimum value for $\Delta^* = \sqrt{N}\Phi$. Then it increases linearly with Δ.

According to Eq.(14), quantum interferences yield holes in the curve $P_{max}(\Delta)$ provided that the relevant Bohr frequencies satisfy the relation $p\varpi_1(\Delta) = q\varpi_2(\Delta)$, where p and q are two integers with opposite parity. For instance, with $N = 16$, $q = 1$ and $p = 2$, a hole $P_{max} = 75.20\%$ occurs for $\Delta = 3.293\Phi$ (see Fig. 9a). Note that the same hole arises for $q = 2$ and $p = 1$ but for $\Delta = 4.707\Phi$. By contrast, P_{max} reaches unity when constructive interferences take place, that is when the relevant Bohr frequencies satisfy the relation $p\varpi_1 = q\varpi_2$, where p and q are two odd integers. In that case, $P_{max} = 1$ occurs at a time $t_{max} = p\pi/\varpi_2 = q\pi/\varpi_1$. For instance, with $N = 16$, $p = 3$, $q = 5$ and $\Delta = 4.516\Phi$, the success probability reaches unity for $t_{max} = 12.16\Phi^{-1}$.

In that context, the key point is that t_{max} can be minimized to ensure a very fast and perfect transfer between the input site and the target site. Such an optimization takes place at the critical point that corresponds to the specific situation for which $p = q = 1$ and $\varpi_1 = \varpi_2$. According to Eq.(12), the critical point arises at the resonance, that is when $\Delta = \Delta^* = \sqrt{N}\Phi$ so that the Bohr frequencies verify $\varpi_1 = \varpi_2 = \Phi$. In that case, the success probability is expressed as $P_{fi}(t) = \sin^4(\Phi t/2)$. As a result, the time for which the exciton reaches the target site with a probability equal to unity reduces to $t^* = \pi/\Phi$, in a quite good agreement with the numerical results displayed in Fig. 8b.

4.3.2 Exact results

As shown previously, when one neglects the influence of the star state $|\chi_-\rangle$, the critical point corresponds to the resonance between the defect states and the star state $|\chi_+\rangle$. In that case, specific quantum interferences arise because the two relevant Bohr frequencies of the system become identical, resulting in a fast and

efficient transfer between the input site and the target site. In a general way, the numerical results displayed in Figs. 7 and 8 show that similar effects occurs when the influence of the star state $|\chi_-\rangle$ is taken into account but with a slightly different critical Δ value. To explain this difference, one proceeds as follows.

After studying numerically the spectrum of the restricted Hamiltonian $\mathcal{H}$ Eq.(5), we have observed that the coupling between the defect states and the star state $|\chi_-\rangle$ only slightly modifies the eigenvalues $\hat{\omega}_1 < \hat{\omega}_2 < \hat{\omega}_3 < \hat{\omega}_4$ provided that $\Delta \approx \sqrt{N}\Phi$. Therefore, one can still assume that a fast and efficient transfer will arises if the two relevant Bohr frequencies $\varpi_1 = \hat{\omega}_3 - \hat{\omega}_2$ and $\varpi_2 = \hat{\omega}_4 - \hat{\omega}_3$ are identical. After straightforward calculations, it turns out that this particular situation occurs provided that Δ reaches a critical value equal to $\Delta^* = \sqrt{N+1}\Phi$. At this critical point, the restricted Hamiltonian $\mathcal{H}$ can be diagonalized exactly. Its eigenvalues are expressed as

$$\begin{aligned}
\hat{\omega}_1 &= -\Delta^* \\
\hat{\omega}_2 &= \Delta^* - \Phi \\
\hat{\omega}_3 &= \Delta^* \\
\hat{\omega}_4 &= \Delta^* + \Phi
\end{aligned} \tag{15}$$

Note that the relevant Bohr frequencies satisfy $\varpi_1 = \varpi_2 = \Phi$, as when we have neglected the coupling with $|\chi_-\rangle$. The corresponding exact eigenvectors are defined as

$$\begin{aligned}
|\Psi_1\rangle &= \frac{1}{\sqrt{6+8N}}\left(|i\rangle - \frac{\sqrt{2}(|\chi_+\rangle + |\chi_-\rangle)}{\sqrt{N+1}+\sqrt{N}} + |f\rangle\right) \\
|\Psi_2\rangle &= \sqrt{\frac{N+2-2\sqrt{N+1}}{4N+6-6\sqrt{N+1}}}\left(|i\rangle + \frac{\sqrt{2}(|\chi_+\rangle + |\chi_-\rangle)}{\sqrt{N+1}-1-\sqrt{N}} + |f\rangle\right) \\
|\Psi_3\rangle &= \frac{1}{\sqrt{2}}\left(|i\rangle - |f\rangle\right) \\
|\Psi_4\rangle &= \sqrt{\frac{N+2+2\sqrt{N+1}}{4N+6+6\sqrt{N+1}}}\left(|i\rangle + \frac{\sqrt{2}(|\chi_+\rangle + |\chi_-\rangle)}{\sqrt{N+1}+1+\sqrt{N}} + |f\rangle\right)
\end{aligned} \tag{16}$$

In that context, from Eqs. (15) and (16), we are able to build the exact expression of the evolution operator Eq.(7) at the critical point. The probability amplitude to observe the exciton on the target site f at time t provided that it was on the excited site i at time $t = 0$ is thus written as

$$\begin{aligned}
U_{fi}(t) = -\frac{1}{2}e^{-i\Delta^* t}\left(1 - \frac{N+2-2\sqrt{N+1}}{2N+3-3\sqrt{N+1}}e^{+i\Phi t} - \frac{N+2+2\sqrt{N+1}}{2N+3+3\sqrt{N+1}}e^{-i\Phi t}\right) \\
+ \frac{1}{8N+6}e^{i\Delta^* t}
\end{aligned} \tag{17}$$

The transition amplitude is the sum over the four elementary amplitudes associated to the four paths that the exciton can follow to tunnel from the input site to the target site. The first term in the right-end-side of Eq.(17) thus refer to the three paths where the transition is mediated by the eigenstates $|\Psi_\alpha\rangle$, with $\alpha = 2$, 3 and 4. These corresponding amplitudes are basically those discussed in the previous section. By contrast, the last term in the right-end-side of Eq.(17)

characterizes the path that involves the state $|\Psi_1\rangle$. This state basically corresponds to $|\chi_-\rangle$ so that the corresponding amplitude yields a quite small correction to the full transition amplitude.

In the limit $N \to \infty$, this latter amplitude vanishes so that one recovers the results established in the previous section. The transfer is thus optimized when the probability amplitudes associated to $|\Psi_2\rangle$ and $|\Psi_4\rangle$ are in phase one with the other and if they are simultaneously in phase opposition with the amplitude associated to $|\Psi_3\rangle$. The shortest time for which such a situation occurs is $t^* = \pi/\Phi$, the resulting success probability being equal to unity. For finite N values, the same argument can be invoked to assume that a fast and efficient transfer arises. Therefore, if one fixes the time to $t^* = \pi/\Phi$, the general expression of the probability amplitude can be determined, giving rise to the optimized success probability defined as

$$P^*(N) = \frac{1}{2}\left[1 + \left(\frac{8N+4}{8N+6}\right)^2\right] - \frac{1}{2}\left[1 - \left(\frac{8N+4}{8N+6}\right)^2\right]\cos(2\sqrt{N+1}\pi) \qquad (18)$$

At the critical point, i.e. when $\Delta = \sqrt{N+1}\Phi$, the N dependence of both the optimized success probability $P^*(N)$ and the optimized transfer time t^* are shown in Fig. 8 (red dashed curves). In a quite good agreement with the numerical results, the curve $P^*(N)$ exhibits damped oscillations around an average value that lies just below unity. As N increases, the amplitude of these oscillations decreases indicating that $P^*(N)$ tends to unity when N tends to infinity. In fact, provided that $N \geq 9$, $P^*(N)$ is larger than 96.85% so that at time t^*, the transition of the exciton from the input site to the target site is a very likely event. This very short time depends only on the hopping constant between the connected sites. In fact, since the input site and the target site are separated by a central node, the value $t^* = \pi/\Phi$ represents the shortest time that is physically accessible to the exciton to tunnel.

To conclude, for performing a quantum search on a star graph involving $N+2$ branches, the molecular network must be chemically designed so that the two energetic defects are characterized by the parameter $\Delta = \sqrt{N+1}\Phi$. In that case, we are sure that a very fast efficient excitonic transfer arises between the input site and the target site. Therefore, by performing a measurement of the excitonic quantum state at time $t^* = \pi/\Phi$, we shall find the exciton localized on the target site with a very large success probability. Consequently, the result of this experiment will reveal the identity of the position of the target site, resulting in a fast and successful quantum search whose powerfulness is becoming better and better as N increases.

5 Conclusion

In this paper, a fast and efficient quantum search algorithm was established by using the ability of an exciton to propagate along a star graph. The exciton dynamics is governed by a tight-binding Hamiltonian that formally corresponds to a physical realization of a CTQW. The star graph is formed by $N_0 + 1$ branch sites that encircle a central site. It exhibits two energetic defects where the site energy of the exciton is shifted by an amount Δ. The first defect, whose position is well-defined, denotes the input site. The second defect occupies the target site whose

position is unknown. So defined, the network refers to an input site connected to N_0 output sites that form a database where the target site is a marked item whose unknown position must be find.

To realize this spatial search we have proposed the following quantum protocol. At time $t = 0$, the exciton is created on the input site. As time elapses, it propagates along the star so that the success probability to reach the target site turns on. When the parameter Δ is judiciously chosen, the time evolution of this probability can be controlled by optimizing the quantum interferences that arise between the different paths that the exciton can follow to tunnel from the input site to the target site. Therefore, when $\Delta = \sqrt{N_0}\Phi$, there exists a very short time $t^* \approx \pi/\Phi$ for which the success probability becomes quite important resulting in a fast and efficient excitonic transfer from the input site to the target site. A measurement of the excitonic quantum state is finally performed at time t^*. The result of the measurement will find the exciton localized on the target site, hence revealing the identity of its position. The key point is that t^* is the shortest time that is physically accessible to the exciton to tunnel. It is N_0 independent so that the powerfulness of the protocol is getting better and better as the size of the database increases.

In the present work, the proposed quantum search algorithm was applied to a very simple star graph. Although a quite powerfulness algorithm was obtained, additional studies are required to investigate what happens in more intricate situations. For instance, it could be wise to consider more complex graphs such as stars of connected star graphs and binary trees. Moreover, from a physical point of view, the exciton does not propagate freely but it interacts with its surrounding that favors energy relaxation and/or dephasing. These effects must be included in our formalism to establish a more general protocol able to operate at finite temperature.

References

1. Feynman, R.: Simulating physics with computers. Int. J. Theor. Phys. **21**, 467 (1982)
2. Deutsch, D.: Quantum theory, the Church-Turing principle and the universal quantum computer. Proc. R. Soc. London A **400**, 97 (1985)
3. Shor, P.W.: Algorithms for quantum computation discrete log and factoring. Proceedings of the 35th Annual Symposium on the Foundations of Computer Science, Los Alamos, pp. 20 (1994)
4. Shor, P.W.: Polynomial-Time algorithms for prime factorization and discrete logarithms on a quantum Computer. SIAM J. Comput. **26**, 1484 (1997)
5. Grover, L.K.: A fast quantum mechanical algorithm for database search. Proceedings of the 28th Annual ACM Symposium on the Theory of Computing, pp. 212-219 ACM press, New York (1996)
6. Grover, L.K.: Quantum mechanics helps in searching for a needle in a haystack. Phys. Rev. Lett. **79**, 325 (1997)
7. Roland J., Cerf N.J.: Quantum search by local adiabatic evolution. Phys. Rev. A **65**, 042308 (2002)
8. Dowling J.P.: Quantum information: To compute or not to compute?. Nature (London) **439**, 919 (2006)
9. Daems D. Guerin S.: Adiabatic Quantum Search Scheme With Atoms In a Cavity Driven by Lasers. Phys. Rev. Lett. **99**, 170503 (2007)
10. Farhi, E., Gutmann, S.: Analog analogue of a digital quantum computation. Phys. Rev. A **57**, 2403 (1998)
11. Childs, A.M., Goldstone, J.: Spatial search by quantum walk. Phys. Rev. A **70**, 022314 (2004)

12. Shenvi, N., Kempe, J., Whaley, K.B.: Quantum random-walk search algorithm. Phys. Rev. A **67**, 052307 (2003)
13. Szegedy, M.: Quantum Speed-Up of Markov Chain Based Algorithms. Proceedings of the 45th IEEE Symposium on Foundations of Computer Science p. 32. IEEE Computer Society, Washington DC (2004)
14. Ambainis, A., Kempe, J., Rivosh, A.: Coins make quantum walks faster. Proceedings of the 16th ACM-SIAM Symposium on Discrete Algorithms p. 1099. Society for Industrial and Applied Mathematics, Philadelphia (2005)
15. Santha, M.: Quantum walk based search algorithms, Proceedings of the Fifth International Conference on Theory and Applications of Models of Computation, TAMC 2008, Xi'an, China, 2008, edited by M. Agrawal, D.-Z. Du, Z. Duan, and A. Li, Lecture Notes in Computer Science p. 31. Springer, Berlin, Heidelberg (2008)
16. Reitzner, D., Hillery, M., Feldman, E., Buzek, V.: Quantum searches on highly symmetric graphs. Phys. Rev. A **79**, 012323 (2009)
17. Kahou M.E., Feder, D.L.: Quantum search with interacting Bose-Einstein condensates. Phys. Rev. A **88**, 032310 (2013)
18. Kahou, M.E.: Spatial search via non-linear quantum walk. PhD Thesis, Department of Physics and Astronomy, Calgary (2013)
19. Merris R.: Laplacian matrices of graphs: A survey. Linear Algebra Appl. **197198** 143 (1994)
20. Agliari,E., Blumen, A., Mulken, O.: Quantum-walk approach to searching on fractal structures. Phys. Rev. A **82**, 012305 (2010)
21. Thilagam, A.: Grover-like search via Frenkel-exciton trapping mechanism. Phys. Rev. A **81**, 032309 (2010)
22. Pouthier, V.: Vibrational exciton mediated quantum state transfer: Simple model. Phys. Rev. B **85**, 214303 (2012)
23. Pouthier, V.: Vibrons in finite size molecular lattices: a route for high-fidelity quantum state transfer at room temperature. J. Phys.: Condens. Matter **24**, 445401 (2012)
24. Mulken, O., Bierbaum, V., Blumen, A.: Coherent exciton transport in dendrimers and continuous-time quantum walks. J. Chem. Phys. **124**, 124905 (2006)
25. Mulken, O., Blumen, A.: Continuous-time quantum walks: Models for coherent transport on complex networks. Phys. Rep. **502**, 37 (2011)
26. Pouthier, V.: Exciton localization-delocalization transition in an extended dendrimer. J. Chem. Phys. **139**, 234111 (2013)
27. Pouthier, V.: Disorder-enhanced exciton delocalization in an extended dendrimer. Phys. Rev. E **90**, 022818 (2014)
28. Pouthier, V.: The excitonic qubit on a star graph: dephasing-limited coherent motion. Quantum Inf. Process **14**, 491 (2015)
29. Salimi, S.: Continuous-time quantum walks on star graphs. Ann. Phys.**324**, 1185 (2009)
30. Xu, X.P.: Exact analytical results for quantum walks on star graphs. J. Phys. A: Math. Theor. **42**, 115205 (2009)
31. Ziletti, A., Borgonovi, F., Celardo, G.L., Izrailev, F.M., Kaplan, L., Zelevinsky, V. G.: Coherent transport in multibranch quantum circuits. Phys. Rev. B **85**, 052201 (2012)
32. Anishchenko, A., Blumen, A., Mulken, O.: Enhancing the spreading of quantum walks on star graphs by additional bonds. Quantum Inf. Process **11**, 1273 (2012)
33. Xu, X.P.: Coherent exciton transport and trapping on long-range interacting cycles. Phys. Rev. E **79**, 011117 (2009)
34. Mulken, O., Blumen, A.: Efficiency of quantum and classical transport on graphs. Phys. Rev. E **73**, 066117 (2006)
35. Wagner M.: Unitary Transformations in Solid State Physics. North-Holland, Amsterdam (1986)
36. Cohen-Tannoudji, C., Dupont-Roc, J., Grynberg, G.: Atom-Photon Interactions : Basic Processes and Applications. Wiley, New-York (1992)